J|A|C|S
ARTICLES
Published on Web 05/25/2004

The Epitaxial Growth of Cholesterol Crystals from Bile Solutions on Calcite Substrates

M. Crina Frincu,[†] Sean D. Fleming,[‡] Andrew L. Rohl,*[,‡] and Jennifer A. Swift*[,†]

Contribution from the Department of Chemistry, Georgetown University, 37th and "O" Streets NW, Washington, DC 20057-1227, and Nanochemistry Research Institute, Curtin University of Technology, GPO Box U 1987, Perth, Western Australia 6845

Received March 2, 2004; E-mail: jas2@georgetown.edu

Abstract: Epitaxial relationships between the surfaces of inorganic and bioorganic crystals can be an important factor in crystal nucleation and growth processes in a variety of biological environments. Crystalline cholesterol monohydrate (**ChM**), a constituent of both gallstone and atherosclerotic plaques, is often found in association with assorted mineral phases. Using in situ atomic force microscopy (AFM) and well-characterized model bile solutions, the nucleation and epitaxial growth of **ChM** on calcite ($10\bar{1}4$) surfaces in real-time is demonstrated. The growth rates of individual cholesterol islands formed on calcite substrates were determined at physiological temperatures. Evidence of Ostwald's ripening was also observed under these experimental conditions. The energetics of various ($10\bar{1}4$) calcite/(001) **ChM** interfaces were calculated to determine the most stable interfacial structure. These simulations suggest that the interface is fully hydrated and that cholesterol hydroxyl groups are preferentially positioned above carbonate ions in the calcite surface. This combination of experimental and theoretical work provides a clearer picture of how preexisting mineral seeds might provide a viable growth template that can reduce the energetic barrier to cholesterol nucleation under some physiological conditions.

Introduction

The deposition of cholesterol crystals in vivo is an undesirable crystallization process that is implicated in a variety of human diseases including the formation of gallstones and atherosclerotic plaques. Although the detailed step-by-step formation of these entities is not yet fully understood, the nucleation of cholesterol crystals is regarded as an important first step in the formation of these pathogenic deposits. Free cholesterol has extremely low solubility in pure aqueous solutions ($\sim 3 \times 10^{-8}$ mol/L, at 30 °C),[1] and only slightly higher solubility in dilute bile salt solutions ($\sim(1-3) \times 10^{-3}$ mol/L, at 35 °C).[2] However, the presence of phospholipids (usually phosphatidylcholine) or other detergents drastically increases the solubility of cholesterol by enabling it to form vesicles or mixed micelle solutions ($\sim$7 g/L at 37 °C).[3] Previous studies using cryo-transmission electron microscopy,[4,5] light microscopy,[6] and synchrotron X-ray diffraction[7] have been used to characterize the evolution of vesicular microstructures in well-characterized model bile and gallbladder bile solutions. In these bile systems, the aggregation and fusion of cholesterol-rich vesicles is generally thought to facilitate nucleation.

Interestingly, a number of clinical studies have demonstrated that cholesterol supersaturation is not the sole prerequisite for **ChM** crystal deposition.[8,9] Some patients with high cholesterol levels that meet the supersaturation conditions do not develop gallstones, while others who do not meet the prerequisite saturation levels can exhibit cholesterol deposits. This clinical evidence suggests that the presence of nucleating or antinucleating agents may also play a fundamental role in the cholesterol nucleation and/or growth processes under biological conditions. Although it is not known exactly which molecules might regulate cholesterol crystallization in vivo, a number of studies have examined the effect of soluble species such as mucin,[10] proteins,[11,12] phospholipids,[13,14] monoclonal antibodies,[15] and metal ions[16,17] on the cholesterol nucleation and growth rates.

[†] Georgetown University.
[‡] Curtin University of Technology.

(1) Saad, H. Y.; Higuchi, W. I. *J. Pharm. Sci.* **1965**, *54*, 1205−1206.
(2) Corradini, S. G.; Elisei, W.; Giovannelli, L.; Ripani, C.; Guardia, P. D.; Corsi, A.; Cantafora, A.; Capocaccia, L.; Ziparo, V.; Stipa, V.; Chirletti, P.; Caronna, R.; Lomanto, D.; Attili, A. F. *Gastroenterology* **2000**, *118*, 912−920.
(3) Small, D. M. *Proc. Natl. Acad. Sci U.S.A.*. **2003**, *100*, 4−6.
(4) Konikoff, F. M.; Danino, D.; Weihs, D.; Rubin, M.; Talmon, Y. *Hepatology* **2000**, *31*, 261−268.
(5) Kaplun, A.; Talmon, Y.; Konikoff, F. M.; Rubin, M.; Aitan, A.; Tadmor, M.; Lichtenberg, D. *FEBS Lett.* **1994**, *340*, 78−82.
(6) Wang, D.; Carey, M. *J. Lipid Res.* **1996**, *37*, 2539−2549.
(7) Somjen, G. J.; Lipka, G.; Schulthess, G.; Koch, M. H. J.; Wachtel, E.; Gilat, T.; Houser, H. *Biophys. J.* **1995**, *68*, 2342−2349.
(8) Admirand, W. H.; Small, D. M. *J. Clin. Invest.* **1968**, *47*, 1043−1052.
(9) Whiting, M. J.; Watts, J. M. *Clin. Sci.* **1985**, *68*, 589−596.
(10) Levy, P. F.; Smith, B. F.; LaMont, J. T. *Gastroenterology* **1984**, *87*, 270−275.
(11) Harvey, P. R. C.; Upadhya, G. A.; Strasberg, S. M. *J. Biol. Chem.* **1992**, *266*, 13996−14003.
(12) Kibe, A.; Holzbach, R. T.; LaRusso, N. F.; Mao, S. J. *Science* **1984**, *225*, 514−516.
(13) Lafont, S.; Rapaport, H.; Somjen, G. J.; Renault, A.; Howes, P. B.; Kjaer, K.; Als-Nielsen, J.; Leiserowitz, L.; Lahav, M. *J. Phys. Chem. B* **1998**, *102*, 761−765.
(14) Rapaport, H.; Kuzmenko, I.; Lafont, S.; Kjaer, K.; Howes, P. B.; Als-Nielsen, J.; Lahav, M.; Leiserowitz, L. *Biophys. J.* **2001**, *81*, 2719−2736.
(15) Perl-Treves, D.; Kessler, N.; Izhaky, D.; Addadi, L. *Chem. Biol.* **1996**, *3*, 567−577.
(16) Toor, E. W.; Evans, D. F.; Cussler, E. L. *Proc. Natl. Acad. Sci. U.S.A.* **1978**, *75*, 6231−6234.

Somewhat less attention has been paid to the potential effects of insoluble species that may also exist under physiological conditions and influence cholesterol crystallization. Compositional analyses of human gallstones have established the presence of a number of calcium carbonate and calcium phosphate phases.[18−20] Although the primary component of most human gallstones is cholesterol (∼80 wt %), the calcium carbonate (∼15 wt %) and calcium phosphate (∼3 wt %) content can also be quite significant.[20] These mineral phases are often found in the central nidius of the stone as well as radially distributed in the successive outer rings.[21] Heterogeneous nucleation is generally considered to be energetically more favorable than homogeneous nucleation, and the presence of an epitaxial surface can reduce the nucleation barrier such that crystal growth can occur in solutions that have otherwise not met supersaturation conditions. Epitaxy is defined as the growth of one crystal on the substrate of another, such that there is at least one preferred orientation and a near geometrical fit between the contacting surface lattices. That these mineral phases frequently coexist with cholesterol deposits suggests a synergistic influence of one crystalline phase on the other may be an important factor in nucleation and growth under physiological conditions.

Crystalline cholesterol deposited under physiological conditions is typically in the form of cholesterol monohydrate (**ChM**).[22] **ChM** crystals grown from bile solutions or from aqueous alcohol solutions consistently develop a similar platelike morphology in which the largest face is (001).[23] The plates are usually bounded by smaller (100), (011), and (010) side faces, and often exhibit a small ($0\bar{1}1$) notch. The deposition of metastable crystalline intermediates including anhydrous cholesterol[24] and/or polymorphs of unknown structure[25] may also precede **ChM** formation under some conditions.

Previously in our laboratory, the geometric lattice-matching program EpiCalc[26] was used as a systematic screening tool to identify which of the low index faces of anhydrous cholesterol and **ChM** are epitaxially matched with the naturally abundant faces of calcium carbonate (calcite, vaterite, aragonite) and calcium phosphate (hydroxyapatite, brushite).[27] For molecular crystal systems, which often contain many molecules per unit cell, simple geometric matching can be performed in a reasonable amount of time and has been shown in many cases to give predictions similar to those of the more rigorous potential energy calculations.[28,29] Our geometric screening protocol predicted 186 coincident epitaxial relationships between the surfaces of these cholesterol and mineral phases, 31 of which were between various combinations of calcite and **ChM** surfaces. By far, the best geometric lattice match was found between the largest (001) plate-face of **ChM** and the natural ($10\bar{1}4$) cleavage face of calcite when the two surfaces are rotated by an azimuthal angle of 39°.

In the present study, we demonstrate experimentally the nucleation and epitaxial growth of ChM from model bile solutions on calcite ($10\bar{1}4$) using in situ atomic force microscopy (AFM) under physiological temperature. The time-resolved data generated in this AFM study confirm the earlier EpiCalc predictions. As geometric matching alone does not provide any information about the molecular structure of the interface or its energetics, we have also undertaken more rigorous molecular simulations of the cholesterol−calcite interface. These calculations involve optimizing slabs of cholesterol with different terminations on the calcite basal plane, which yield not only the most stable interface but also information on the intermolecular interactions that direct the precise positioning of the contacting crystal surfaces. This dual approach affords a more detailed nanoscale understanding of how mineral seeds may have a profound effect on cholesterol crystallization in vivo.

Experimental Section

Materials. High purity cholesterol (Aldrich, 99+%) and sodium taurocholate (**TC**) (Sigma, 97%) were used without further purification. Egg yolk phosphatidyl choline (**PC**) in chloroform solution (20 mg/mL) was purchased from Avanti Polar-Lipids (Alabaster, AL). Calcite was purchased from the Smithsonian Museum of Natural History (Washington, DC). Water was purified by passage through two Barnstead deionizing cartridges followed by distillation. All glassware was cleaned with an alcohol−alkali solution (ethanol:KOH 1:1 vol), acid washed (1 M HNO_3) and thoroughly rinsed with deionized distilled water, wrapped in aluminum foil, and oven dried before use.

Model Bile Solution. Model bile solutions mimicking human gallbladder bile were prepared according to the system developed by Konikoff et al.[4,30] Stock solutions of 99+% cholesterol (in methanol), **PC** (in chloroform), and **TC** (in methanol) were mixed in a molar ratio of 18:37:120 and subsequently dried under nitrogen and low vacuum for 18 h to form a lipid film. Resuspension of the film in an aqueous solution containing 0.15 M NaCl and 0.003 M sodium azide (an antimicrobial agent) and heating to 56 °C for 1 h yielded a concentrated lipid solution (90 g/dL). The solution was diluted with additional 0.15 M NaCl to yield a total lipid concentration of 10 g/dL and was maintained at 37 °C in a water bath for a period of 21 days. The turbidity of the solution appeared to increase over days 1−10, then slowly decreased over time until day 21, at which time a white precipitate containing **ChM** crystals had completely separated from the clear yellowish supernatant. Small aliquots of the clear supernatant were removed with a disposable Pasteur pipet, transferred onto a glass microscope slide, and examined under polarized optical microscopy. Aliquots free of visible particulates were removed from the solution and used in AFM experiments without any further processing.

Cholesterol Monohydrate Crystal Growth. Cholesterol monohydrate crystals were grown both from model bile solutions as described above and from the slow evaporation of supersaturated aqueous acetone or 95% ethanol solutions. Optical micrographs obtained on an Olympus BX50 microscope of bile-grown and conventional solvent-grown **ChM** crystals reveal that they are identical morphologically. Single **ChM** crystals selected for AFM imaging studies were those that appeared to have the smoothest surfaces under optical microscopy.

Substrate Preparation. Calcite has a natural cleavage plane along ($10\bar{1}4$). Fresh ($10\bar{1}4$) surfaces of calcite were cleaved immediately prior

(17) Moore, E. W. *Hepatology* **1990**, *12*, 206S−226S.
(18) Malet, P. F.; Dabezies, M. A.; Huang, G.; Long, W. B.; Gadacz, T. R.; Soloway, R. D. *Gastroenterology* **1988**, *94*, 1217−1221.
(19) Nagpal, K. C.; Ghori, T. A.; Ali, S. Z. *Curr. Sci.* **1982**, *51*, 814−815.
(20) Bogren, H. G.; Mutvei, H.; Renberg, G. *Ultrastruct. Pathol.* **1995**, *19*, 447−453.
(21) van der Berg, A. A.; van Buul, J. D.; Tytgat, G. N. J.; Groen, A. K.; Ostrow, J. D. *J. Lipid Res.* **1998**, *39*, 1744−1751.
(22) Craven, B. M. *Nature* **1976**, *260*, 727−729.
(23) Abendan, R. S.; Swift, J. A. *Langmuir* **2002**, *18*, 4847−4853.
(24) Shieh, H. S.; Hoard, L. G.; Nordman, C. E. *Nature* **1977**, *267*, 287−289.
(25) Konikoff, F. M.; Chung, D. S.; Donovan, J. M.; Small, D. M.; Carey, M. C. *J. Clin. Invest.* **1992**, *90*, 1155−1160.
(26) Hillier, A.; Ward, M. D. *Phys. Rev. B* **1996**, *54*, 14037−14051.
(27) Frincu, M. C.; Sharpe, R. E.; Swift, J. A. *Cryst. Growth Des.* **2004**, *4*, 223−226.
(28) Hooks, D. E.; Fritz, T.; Ward, M. D. *Adv. Mater.* **2001**, *13*, 227−241.
(29) Last, J. A.; Hooks, D. E.; Hillier, A. C.; Ward, M. D. *J. Phys. Chem.* **1999**, *103*, 6723−6733.
(30) Konikoff, F. M.; Laufer, H.; Messer, G.; Gilat, T. *J. Hepatol.* **1997**, *26*, 703−710.

to AFM experiments. Contact-mode imaging of freshly cleaved calcite surfaces reveals well-defined and oriented facets, which are easily distinguishable from the surface topography of cholesterol monohydrate crystals.

Atomic Force Microscopy (AFM). All real-time cholesterol growth studies were performed on a Nanoscope IIIa atomic force microscope (Digital Instruments, Santa Barbara, CA) equipped with Nanoscope III 4.43r8 software, an E-scanner (17.4 μm^2 max. area), and Si_3N_4 tips with a force constant of 0.12 N/m. The AFM is also equipped with a temperature stage (DI Metrology Group Heater Controller, model HS-1), which allows for heating from room temperature to 50 °C. A custom-built fluid reservoir was designed to precondition the temperature of the bile solution before it enters the 30 μL glass fluid cell. The fluid was introduced with a 10 mL Hamilton syringe (model 81620); a syringe pump (KD Scientific 200) was used to regulate the flow rate (between 0.5 and 4 mL/h) through the fluid cell.

Calcite and cholesterol crystal samples were mounted to a metallic sample puck with double sided tape or with a mixture of 5 min epoxy/5 min epoxy hardener (Devcon, ITW Brands). Except in control experiments, calcite samples were usually oriented such that the *X*-scan axis is parallel to one of the crystal edges. AFM images of calcite $(10\bar{1}4)$ surfaces exposed to aqueous solutions at 37 °C with pH's similar to those of the model bile solutions used did not show any appreciable changes over a period of several hours. Both contact- and tapping-mode techniques were used to image cholesterol and calcite crystals in air and in fluid (model bile solution or pure water) at room temperature and at 37 °C. We note that contact-mode imaging of cholesterol crystals in air often results in tip-induced etching, although contact imaging in solution and/or tapping-mode imaging can usually be performed without evidence of sample surface damage.

Computation and Molecular Simulation. The crystal structure of **ChM** was taken from the work of Craven[22] and the Cerius[2] molecular modeling package[31] was used to add the hydrogen atoms. Visual inspection showed that the added hydrogen atoms were not in the correct orientation to form a hydrogen bonded network in the middle of the cholesterol/water bilayer. Thus, the hydrogen atoms were subjected to 1000 ps of molecular dynamics at 750 K, followed by 250 ps at 298 K after which they were minimized. The timestep used was 1 fs. These calculations utilized the CVFF force field[32] within the Discover molecular simulation program.[33] The van der Waals interactions were cut off after 12 Å, and the electrostatic contribution to the lattice energy was evaluated using the Ewald sum. Each water molecule in the minimized structure was found to form three hydrogen bonds, two with hydroxyl groups on cholesterol molecules and the third with a neighboring water molecule. A CIF file containing the minimized hydrogen coordinates is available as Supporting Information. This model was then fully minimized using the CVFF, CFF91,[34] and ESFF[35] force fields using the same treatment of the long-range potentials in Discover.

The vacuum growth morphology of **ChM** was derived by calculating the unrelaxed attachment energy (E_{att}) of a growth slice of thickness d_{hkl} to the 15 faces with the largest interplanar spacings.[36] The calculations were done using the latest version of GULP,[37] which can simulate surfaces with two-dimensional periodic boundary conditions. This code utilizes a two-region approach, where the top layers of the surface are placed in region I and it is possible for these ions to be relaxed. The ions in region II are kept fixed and represent the potential of the bulk on region I. The CVFF force field was used in these simulations with identical treatment of the long-range interactions as for the Discover simulations above. Note that **ChM** crystallizes in a noncentrosymmetric space group and thus the face (*hkl*) is crystallographically distinct to $(\bar{h}\bar{k}\bar{l})$. However, the unrelaxed attachment energies of these two faces are identical as the growth slices are the same (they are just attached to opposite sides of the crystal), and the sum of the attachment energy and the slice energy is the crystal energy.[38] To determine the possible surface terminations for face (*hkl*), the surface cell is cleaved in the *z* direction. To ensure that complete molecules result from this procedure, the position of each molecule is represented by its centroid. Starting at the origin and moving the cleavage plane by translating it in *z*, a different surface termination will occur when the slice moves from between two neighboring centroids to the next pair of centroids. Thus, in general, the number of possible surface terminations is equal to the number of centroids, unless symmetry is present. In cholesterol, there are 16 molecules (8 cholesterol and 8 water) and no symmetry, so each face has 16 different possible surface terminations. The attachment energies of all 16 were calculated, and the smallest in absolute value was retained because the morphological importance of a face is inversely proportional to the absolute value of the attachment energy. Finally, the calculated morphology is displayed via a Wulff plot.[39]

The energetics of the cholesterol/calcite interactions were determined and subsequently used to provide a nanoscale description of the cholesterol/calcite interface. The interatomic potentials for calcite were taken from our previous work,[40] and the calcite to cholesterol potentials were taken from the ESFF force field. Next, a 2 × 2 supercell of the $(10\bar{1}4)$ calcite cleavage plane with three layers in region II and three layers in region I was constructed. A growth slice of the (001) surface of cholesterol is rotated by 39° and placed in region I above the calcite surface. The growth slice is first kept rigid and allowed to translate in *x*, *y*, and *z* with respect to the fixed calcite surface, until the minimum energy is found. All of the region I ions are then allowed to relax to their minimum energy positions. To try and ensure that the global minimum was found, each growth slice is started from four different starting positions. The first configuration is manually placed at a reasonable position above the surface. This is then translated half a lattice translation of the 1 × 1 $(10\bar{1}4)$ calcite surface cell, first along **a**, then along **b**, and finally along both. Although the (001) growth slice has 16 possible terminations, only 4 of these produce a flat surface, which we have termed hydrophobic, hydrophilic, half water layer, and full water layer. These slices are more stable than the remaining 12 corrugated surfaces and thus are the only ones considered in the interfacial calculations. To assess which configuration is the most favorable, the attachment energy of the cholesterol layer to the calcite was calculated. The attachment energy is defined by:

$$E_{att}^{\text{calcite/cholesterol}} = (E^{\text{calcite+cholesterol}} - E^{\text{calcite}} - E^{\text{cholesterol}})/8$$

where the first term on the right is the minimum energy of the system containing the cholesterol slab on the calcite surface, the second term is the energy of the calcite surface minimized without the cholesterol slab present, and the final term is the energy of the cholesterol slab minimized in the absence of the calcite surface. As there are 8 cholesterol molecules in the slab, the total energy is divided by 8 to yield the attachment energy per molecule. The relaxed attachment energy can also be calculated for the cholesterol slab and a cholesterol surface by repeating the above calculations but replacing the calcite surface with the (001) surface of cholesterol with one layer in region I, and one layer in region II. The GDIS program (http://gdis.sf.net) was used to do all the manipulations required to construct the various interfaces, and the optimizations of these configurations were done using GULP.[37]

(31) *Cerius*^{2}, 4.0 ed.; Accelrys, 1999.
(32) Dauber-Osguthorpe, P.; Roberts, V. A.; Osguthorpe, D. J.; Wolff, J.; Genest, M.; Hagler, A. T. *Proteins: Struct., Func. Genet.* **1988**, *4*, 31−47.
(33) *Discover*, 99.1 ed.; Accelrys, 1999.
(34) Maple, J. R.; Dinur, U.; Hagler, A. T. *Proc. Natl. Acad. Sci. U.S.A.* **1988**, *85*, 5350−5354.
(35) Shi, S. H.; Yan, L.; Yang, Y.; Fisher-Shaulsky, J.; Thacher, T. *J. Comput. Chem.* **2003**, *24*, 1059−1076.
(36) Gay, D. H.; Rohl, A. L. *J. Chem. Soc., Faraday Trans.* **1995**, *91*, 925−936.
(37) Gale, J. D.; Rohl, A. L. *Mol. Simul.* **2003**, *29*, 291−341.
(38) Hartman, P.; Bennema, P. *J. Cryst. Growth* **1980**, *49*, 145−156.
(39) Wulff, G. *Z. Krystallogr.* **1901**, *34*, 449−530.
(40) Rohl, A. L.; Wright, K.; Gale, J. D. *Am. Mineral.* **2003**, *88*, 921−925.

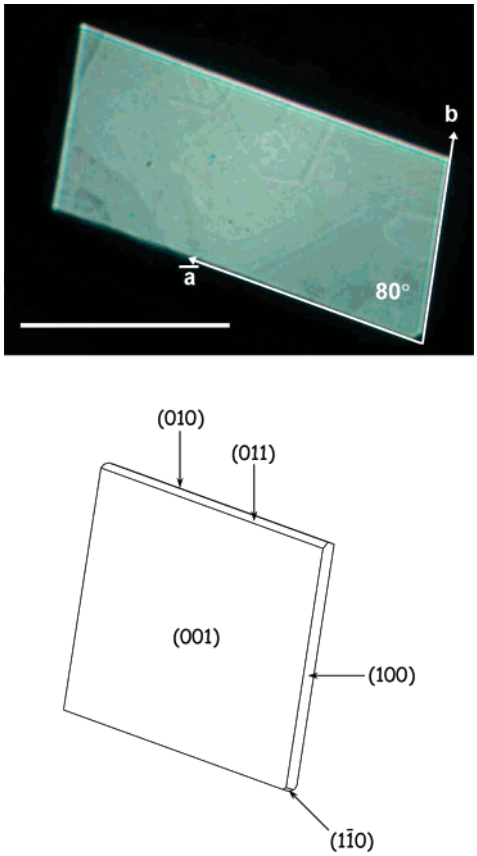

Figure 1. (top) **ChM** plates grown from model bile solution, scale bar = 0.05 mm. (bottom) Theoretical **ChM** morphology.

Results and Discussion

Real-Time Cholesterol Growth on Calcite (10$\bar{1}$4) Substrates. Our experimental epitaxy studies utilize model bile solutions and freshly cleaved calcite surfaces. The model bile used in this work was based on a system developed by Konikoff et al.,[4,30] which has previously been shown via cryo-TEM studies to contain micellar aggregates that are similar to those present in human gallbladder bile solutions. The bile is prepared by mixing three key reagents − cholesterol, phosphatidylcholine, and sodium taurocholate − in an 18:37:120 molar ratio. When a 10 g/dL lipid solution of this composition is maintained at 37 °C, for the initial first 10 days immediately following the solution preparation, the bile solution shows a noticeable increase in turbidity. After that time, the turbidity appears to decrease, and on or about day 21, a white precipitate containing **ChM** crystals separates from the clear yellowish supernatant.

The **ChM** crystals deposited from this solution are clear plates and are typically 0.10 mm in their largest dimension (Figure 1). The acute angle observed between (100) and (010) side faces typically measures 80 ± 0.7°, which is consistent with the expected complement to the known crystallographic angle γ = 100.8°. **ChM** crystals grown from bile solution are morphologically identical to those grown from conventional aqueous alcohol solutions. The calculated theoretical morphology is also a rhombic plate, with the largest (001) face bounded by smaller side (100) and (010) faces with a (011) chamfering face and a very small (1$\bar{1}$0) facet. While the calculated major faces are consistent with the experimental growth morphology, the small (011) and (1$\bar{1}$0) faces are not always observed experimentally, although (1$\bar{1}$0) is clearly visible in the experimental morphology in Figure 1.

The EpiCalc screening procedure utilized in previous work predicted the best epitaxial match to be between calcite (10$\bar{1}$4) and **ChM** (001). We therefore focused our initial experimental studies on calcite (10$\bar{1}$4) substrates. Calcite has a natural cleavage plane along (10$\bar{1}$4); this surface is charge neutral, with an even number of carbonate and calcium groups. Using in situ atomic force microscopy, changes to the calcite surface upon introduction of model bile solutions could be examined in real time. AFM images were collected continuously over a time frame of about 2−3 h, although some experiments involved imaging over longer time periods. Experiments were performed under both dynamic- and static-mode conditions (i.e., with or without flow). The series of images in Figure 2 depict typical changes resulting from the introduction and continuous flow (2 mL/h) of mature 30-day old model bile solution over the calcite (10$\bar{1}$4) surface. Image A is that of calcite in pure aqueous solution. Soon after the bile solution is introduced to the fluid cell, a number of cholesterol islands appear on the surface. Images B (13 min), C (68 min), and D (126 min) are representative images selected from a larger series to illustrate changes to the surface over time. We note that for approximately the first 5−10 min immediately following bile introduction, AFM properties of bile and pure water are sufficiently different that the AFM detector must be realigned once the solutions are exchanged. Only images collected after the initial 10 min blackout period are used for analysis of the cholesterol growth process.

There is substantial evidence to suggest that these islands formed on the calcite surface are **ChM**. The angle made between the side faces of any individual island measures ∼80° throughout the series. None of the other known cholesterol crystal phases, including anhydrous cholesterol,[41] are known to exhibit this angle. Cross-sectional analyses of the island surfaces also reveal molecular-scale steps that have minimum heights of ∼34 Å, a value that matches the expected heights for cholesterol bilayers in **ChM**. AFM images of the earliest islands observed may suggest a morphology that resembles half-pyramids more so than the characteristic plate shape expected of **ChM**. However, the skewed aspect ratio of the islands is due at least in part to the very different horizontal and vertical scales used in presenting these AFM images. After several hours of growth, when the islands are significantly larger, the scale of the AFM images obtained more clearly resembles the plate shape morphology indicative of macroscopic **ChM** crystals (Figure 3).

Figure 3 depicts the theoretical match based on geometric considerations between a 2 × 1 supercell of calcite (10$\bar{1}$4) substrate (with a_1 = 4.989 Å, a_2 = 8.095 Å, a = 90°) and a **ChM** (001) overlayer (with b_1 = 12.39 Å, b_2 = 12.41 Å, β = 100.8°) at an azimuthal rotation angle θ = 39°.[42] In our in situ AFM studies, the calcite substrate is typically positioned such that one of the macroscopic edge faces is parallel to the *X*-scan direction. On the basis of the calcite substrate orientation and

(41) Shieh, H.-S.; Hoard, L. G.; Nordman, C. E. *Acta Crystallogr.* **1981**, *B37*, 1538−1543.
(42) In ref 27, a value of a_2 = 4.047 Å was used in EpiCalc calculations, such that the same lattice match at θ = 39° corresponds to a (2 × 2) supercell. This same geometric match we here refer to as a (2 × 1) supercell with a_2 = 8.095 Å.

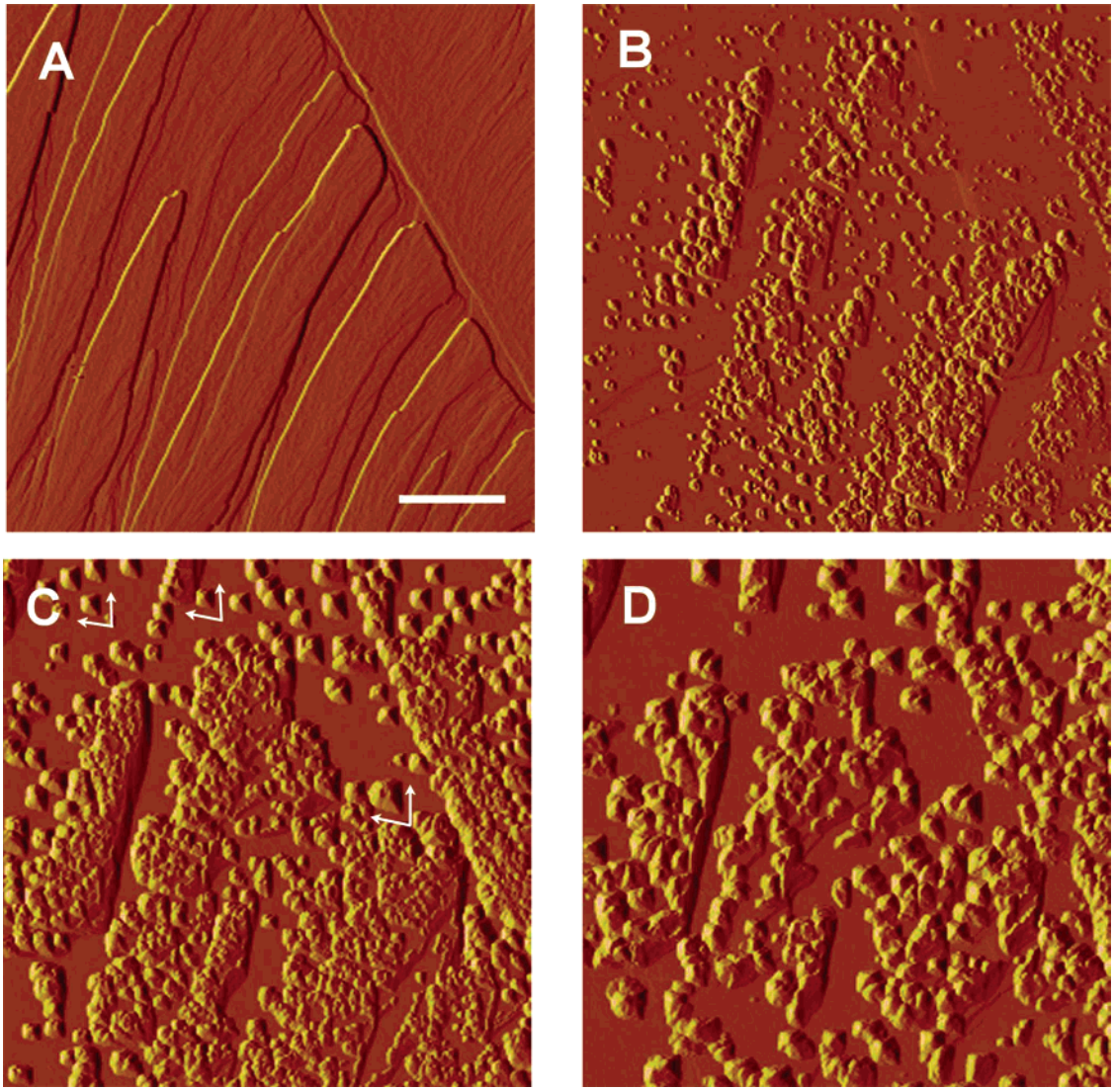

Figure 2. Selected sequential deflection-mode AFM images of the calcite ($10\bar{1}4$) surface before and after exposure to flowing model bile solution. Temperature = 37 °C, pH = 5.4. Image A is a contact-mode image of calcite in water before the introduction of bile solution. Bile solution is introduced to the fluid cell and continuously flowed over the surface at 2 mL/h. Images B, C, and D were obtained 12, 68, and 126 min after initial bile introduction, respectively (scale bar = 2 μm).

the lattice-matching predictions, one would expect the (010) edge of **ChM** islands nucleated and/or grown on these substrates to lie nearly parallel to the *X*-scan direction. Indeed, in every experiment, we find this to be the case. All cholesterol islands observed are aligned relative to one another and to the substrate at the 39° angle predicted by the lattice-matching protocol. The common orientation of islands is indicated in Figures 2c and 3 to show the influence of the underlying epitaxial substrate.

Tracking Individual Island Growth. Surface growth rates can be obtained by different methods. The first method, which yields average growth rates, is based on changes in the surface roughness (R_a) over time, a value that can be readily calculated using standard DI software. Frames A−D in Figure 1 have increasing roughness values ranging from R_a = 0.438 nm (A) for pure calcite, to R_a = 1.633 nm (B), 4.790 nm (C), and 6.621 nm (D) at times after bile is introduced. This type of quick measurement provides at least a qualitative estimate of the growth. A more detailed analysis of individual islands over sequential images is required to determine relative and absolute growth rates as well as any apparent growth anisotropy.

The height, width, and volume of eight individual islands were extracted from sequential AFM images obtained over a 2 h growth experiment. Those islands selected for growth measurements are identified in Figure 4 with white circles. Islands 1−3 appear in the lower left side of the images, while islands 4−8 are in the top central part of the images. Typical islands first observed on the calcite surface are approximately 2500 Å wide by 250 Å high, giving them a cross-sectional volume of 1.6×10^9 Å^3. Using molecular volume estimates based on one-eighth of the **ChM** unit cell volume (5128.193 Å^3),[22] this corresponds to $\sim 2.4 \times 10^6$ molecules of cholesterol per island.

The growth rate of individual islands can be quite variable (Figure 5a). For the eight islands examined, the average growth rate over the course of the experiment ranges between 3×10^5 and 1.4×10^6 molecules/min. Careful tracking of a single island's size over time reveals that the growth rate of any given island is also not uniform over the duration of the experiment; rather, an island can grow much faster or slower than the average at different times. The variability of an island's absolute growth

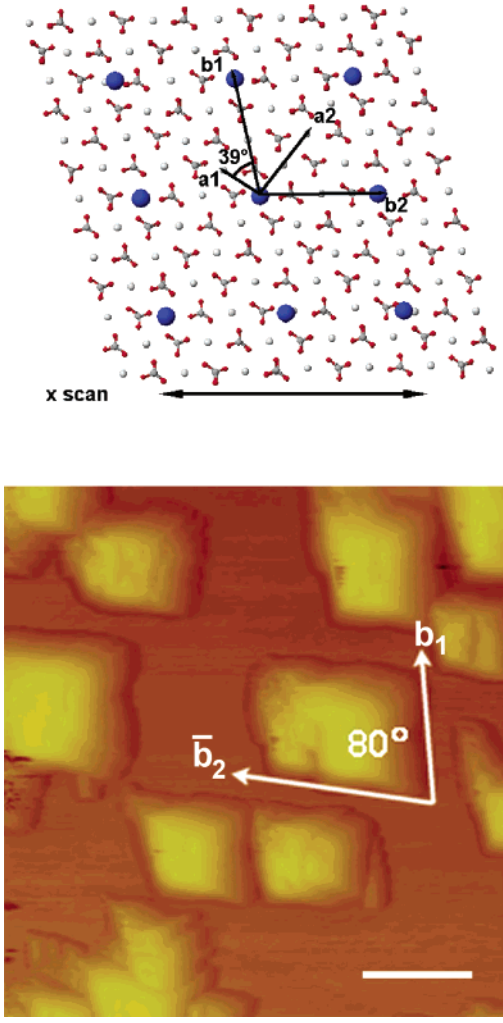

Figure 3. (top) Schematic of the best coincident epitaxial match between calcite (1014) and **ChM** (001) surfaces predicted by geometric lattice matching. The calcite lattice is oriented the same as that in all AFM images presented. (bottom) Tapping-mode AFM images taken after 53 min of growth show platelike **ChM** island morphologies similar to macroscopic crystals. Overlayer cell vectors are indicated (scale bar = 1 μm, z-scale = 800 nm).

rate may be due to a variety of factors. A **ChM** island that resides in an area with a relatively high density of islands might be expected to grow at a slower rate than one in a less dense area, if the growth rate is at all limited by local competition for nutrients. Other factors such as sudden increases in a particular island's surface defect density,[43] the coalescence of multiple islands, and/or local concentration gradients in solution might also contribute to spontaneous changes in the observed growth rates. In a few cases, sudden growth rate changes of islands 1−8 seem to be correlated with other events on the surface. For example, the growth of island 1 increases significantly between $T = 87$ min and $T = 107$ min, while island 2 appears to actually decrease in size over the same time frame. While there is no direct evidence that cholesterol molecules from islands 1 and 2 were exchanged, the islands' close proximity and the timing of the sudden growth rate changes suggest at least qualitatively that local changes in growth rates may be related.

(43) Burton, W. K.; Cabrera, N.; Frank, F. C. *Proc. R. Soc. London, Ser. A* **1951**, *243*, 299−358.

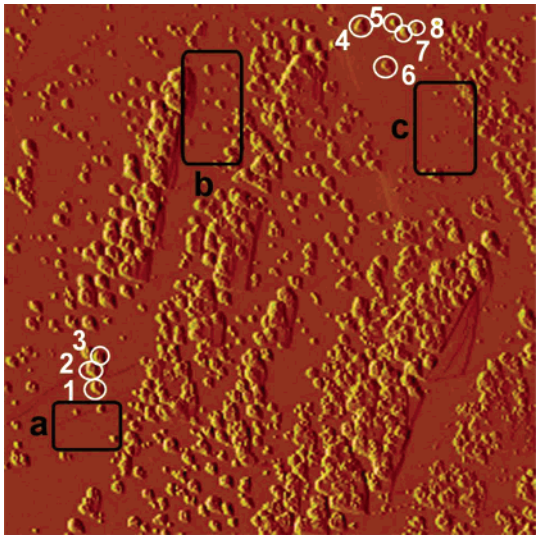

Figure 4. Islands 1−8 circled in white were found to grow both horizontally and vertically over the course of several hours. Black rectangles a−c identify areas where small islands disappeared over the same period of time in which others grow, presumably due to Ostwald's ripening.

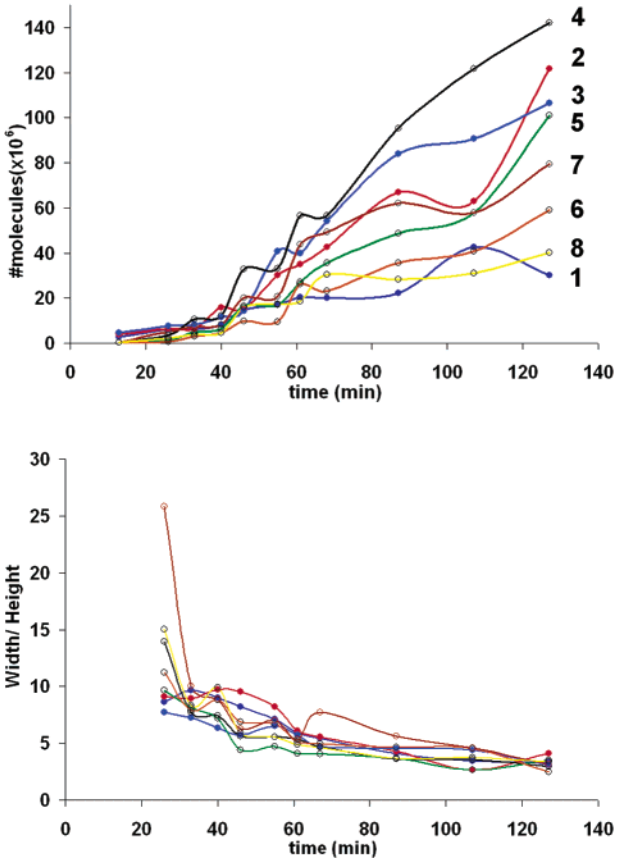

Figure 5. (top) Estimated number of molecules in individual **ChM** islands 1−8 plotted as a function of time. (bottom) The aspect ratio of islands 1−8 during growth plotted as a function of time. Numbers 1−8 correspond to the islands identified in Figure 4.

The growth is also highly anisotropic, as evidenced by the changing relative and absolute aspect ratios (horizontal vs vertical growth) of individual islands. In general, growth parallel to the calcite surface occurs much faster than growth normal to it, which is what one would expect on the basis of the platelike morphology of **ChM**. Interestingly, the aspect ratios of islands

Table 1. Comparison of Experimental and Optimized Cell Parameters Using Three Different Force Fields

	expt[22]	CVFF	CFF91	ESFF
a	12.390	12.510	12.558	12.472
b	12.410	12.112	12.193	12.092
c	34.360	34.959	34.595	34.570
α	91.90	88.47	88.51	88.10
β	98.10	100.93	100.21	100.10
γ	100.80	101.24	102.44	101.53
cell volume	5128.2	5100.3	5090.3	5029.3
deviation (%)		−0.54	−0.74	−1.93

1−8 all decrease over the course of the experiment (Figure 5b). While islands start off with a broad distribution of aspect ratios, after 2 h of growth, most of the islands have attained aspect ratios of ∼5:1 (width:height). In the absence of a substrate, the aspect ratio may be quite different, as macroscopic **ChM** crystals tend to have aspect ratios of ∼15:1.

While there is clear evidence for island growth in both the horizontal and the vertical directions, it can be easy to miss some of the other more subtle changes in the surface topography. In nearly every set of cholesterol growth images collected, careful analysis revealed some evidence for disappearing islands concomitant with the growth of a large majority of islands. Those islands that disappear tend to be among the smallest ones observed (relative to the other islands present on the surface). Three regions marked with black rectangles in Figure 4 identify areas that contain some of the smallest (3×10^8 Å^3) cholesterol islands seen in our AFM bile studies on calcite. Some of the islands in these regions were observed to disappear at different times in the image sequence. For example, islands in box a disappear after the topograph collected at $T = 107$ min. In boxes b and c, some of the islands disappear between $T = 33-40$ min, while others continue to reside in those areas for even longer periods of time. All are gone in the image collected at $T = 127$ min. We surmise that this complex growth and dissolution behavior is clear evidence for an Ostwald ripening process.

From a kinetic standpoint, the formation of many small islands is favored because they nucleate more easily. However, because molecules on the surface of these islands are energetically less stable than those in the interior, larger islands with a smaller surface/volume ratio represent a lower energy state. Thus, in this spontaneous ripening process, small islands can serve as nutrients for the growth of larger islands so that a lower total energy state can be attained. While it can be argued that disappearing islands might also be due to image artifacts, surface ripening was observed in both contact- and tapping-mode imaging with about equal frequency, suggesting that tip-induced shear forces are not a major contributor to this effect. Similarly, rotation of the substrate and/or changing the image scanning direction had no discernible effect.

Molecular Simulation of the Calcite/Cholesterol Interface. Although EpiCalc can determine which facets of **ChM** are likely to grow on calcite substrates and their required orientation, these calculations only take into account geometric factors. Such calculations offer no information about the chemistry of the interface. More rigorous molecular simulations are required if one is to determine which of the possible **ChM** (001) surface terminations are most energetically favorable to bind to the calcite surface. Such calculations also provide a means to assess which calcite−cholesterol interactions direct the precise positioning of the facet, a factor that is critical for determining the position of the supercell's origin.

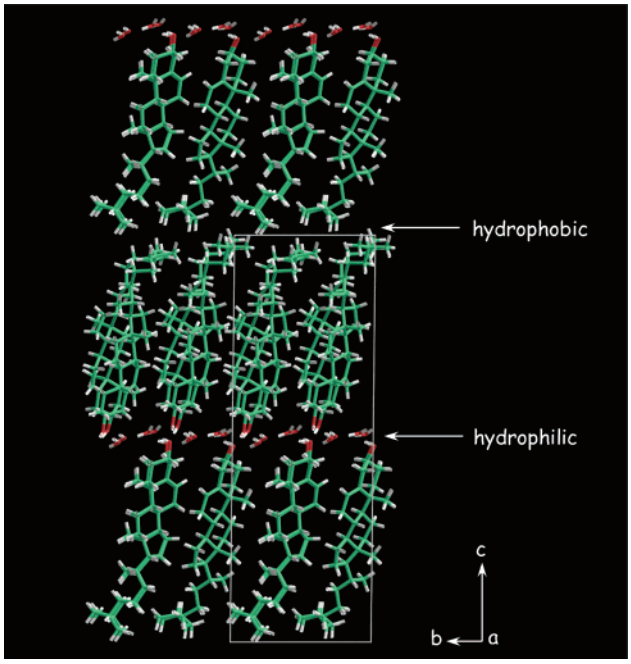

Figure 6. Schematic of hydrophilic versus hydrophobic **ChM** surfaces.

Table 2. Attachment Energies of Cholesterol (001) Growth Slices with Four Different Terminations to Calcite and Cholesterol Surfaces

	(calcite–chol) E_{att} (eV/mol)	(chol–chol) E_{att} (eV/mol)
hydrophobic	−0.16	−0.12
hydrophilic	−0.40	−0.28
hydrophilic + half water	−0.75	−0.35
hydrophilic + full water	−0.84	−0.31

There are two previous molecular modeling studies of the solid-state structures of cholesterol and its derivatives. In the first, Liang and co-workers[44] simulated the condensed phase structures of anhydrous cholesterol and cholesteryl acetate using the CVFF class I force field as well as the CFF91 class II force field. They found that for the structures minimized with the latter force field, all cell vectors and volumes were reproduced to within 2.4% of experimental values and that employing molecular dynamics averaged structures resulted in an even better description. Limited comparisons with the class I force field showed no major differences. Ma et al.[45] used the MM3 class II force field to examine the solid-state structure of cholesteryl acetate and found that the cell vectors and volume were reproduced to within 0.7% as compared to 1.1% for CVFF and 2.1% for CFF91.

The results of our crystal structure optimizations are summarized in Table 1. The magnitude of the changes in lattice parameters is larger than that previously reported for cholesteryl acetate, with a maximum deviation of 2.6% in the cell lengths (ESFF) and larger changes in the angles, particularly α (4.2% for ESFF). What is most surprising is that all three force fields produce very similar cells, with the *a* and *c* axes larger than the experimental structure and the *b* axis smaller. The angles

(44) Liang, C. X.; Yan, L. Q.; Hill, J. R.; Ewig, C. S.; Stouch, T. R.; Hagler, A. T. *J. Comput. Chem.* **1995**, *16*, 883−897.
(45) Ma, B. Y.; Lii, J. H.; Chen, K. S.; Allinger, N. L. *J. Am. Chem. Soc.* **1997**, *119*, 2570−2573.

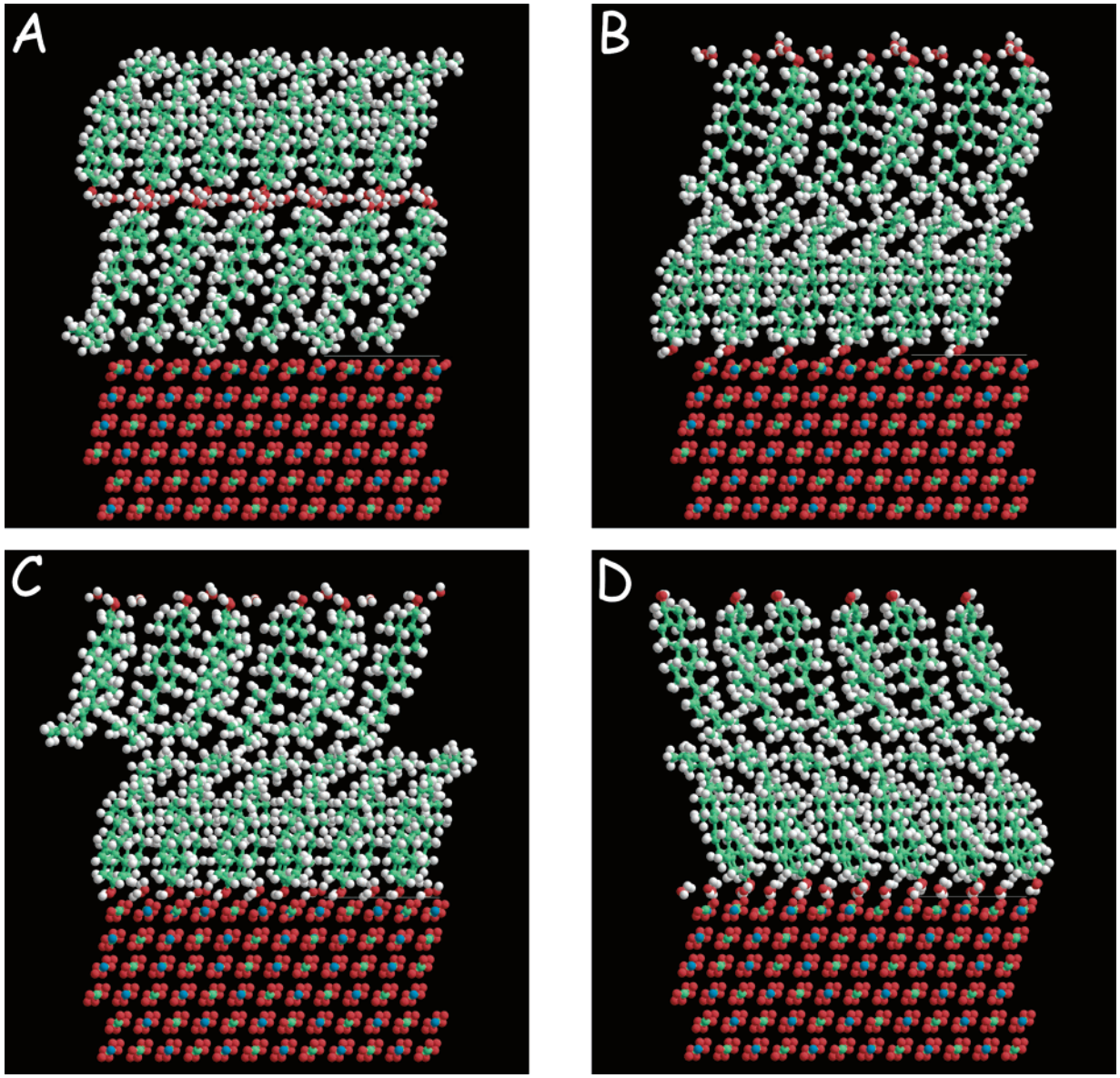

Figure 7. The final optimized configurations for the four different interfaces between **ChM** (001) and calcite ($10\bar{1}4$). A = hydrophobic **ChM**; B = hydrophilic **ChM**; C = hydrophilic **ChM** with a half hydration layer; D = hydrophilic **ChM** with a full hydration layer.

all show similar trends. Visualization of the calculated structures reveals why the calculations deviate from the experimental results. The water−water and water−hydroxyl interactions are stronger in the calculations than in the experimental structure. The water interaction potentials were derived for liquid water, but the layer of water in the middle of the bilayers is not as polarized as liquid water. None of the potentials studied allow for variations in polarizability as a function of environment; thus all of the force fields overbind the water molecules, leading to the differences between the calculated and experimental cells. The CVFF and CFF91 potentials fare better than the ESFF force field. We have utilized the CVFF force field in the surface simulations rather than CFF91, as it is much simpler and thus less computationally demanding.

The unrelaxed attachment energies of the 15 cholesterol faces with the highest interplanar *d* spacings were calculated. The (001) face was found to have a much smaller attachment energy (−0.0669 eV/mol) than all of the other faces. There is a group comprising the (100), (010), (011), and (101) faces which have attachment energies between −0.28 and −0.31 eV/mol, but all of the remaining faces have absolute energies greater than 0.38 eV/mol.[46]

It has been shown that under a given set of solution conditions, the largest plate face of **ChM** may be either hydrophilic with surfaces terminated with 3-hydroxyl groups or hydrophobic exposing the tail groups[23] (Figure 6). The results from docking a cholesterol monohydrate layer with varying surface terminations onto the basal plane of calcite are compared to the values calculated for attaching the same cholesterol monohydrate layer to a **ChM** surface in Table 2. Based on calculations, it appears that more energy is liberated when the cholesterol slice (with any termination) is added to the basal surface of a calcite crystal than when the same slice is added to

(46) $(\bar{h}\bar{k}\bar{l}) = E_{att}$: (10-1) = −0.3892 eV/mol; (100) = −0.2818 eV/mol; (010) = −0.3071 eV/mol; (01-1) = −0.3566 eV/mol; (011) = −0.2940 eV/mol; (10-2) = −0.4855 eV/mol; (101) = −0.2915 eV/mol, (01-2) = −0.4995 eV/mol; (012) = −0.3971 eV/mol; (-111) = −0.4741 eV/mol; (1-10) = −0.4581 eV/mol; (10-3) = −0.5542 eV/mol; (102) = −0.4108 eV/mol; (-112) = −0.5626 eV/mol.

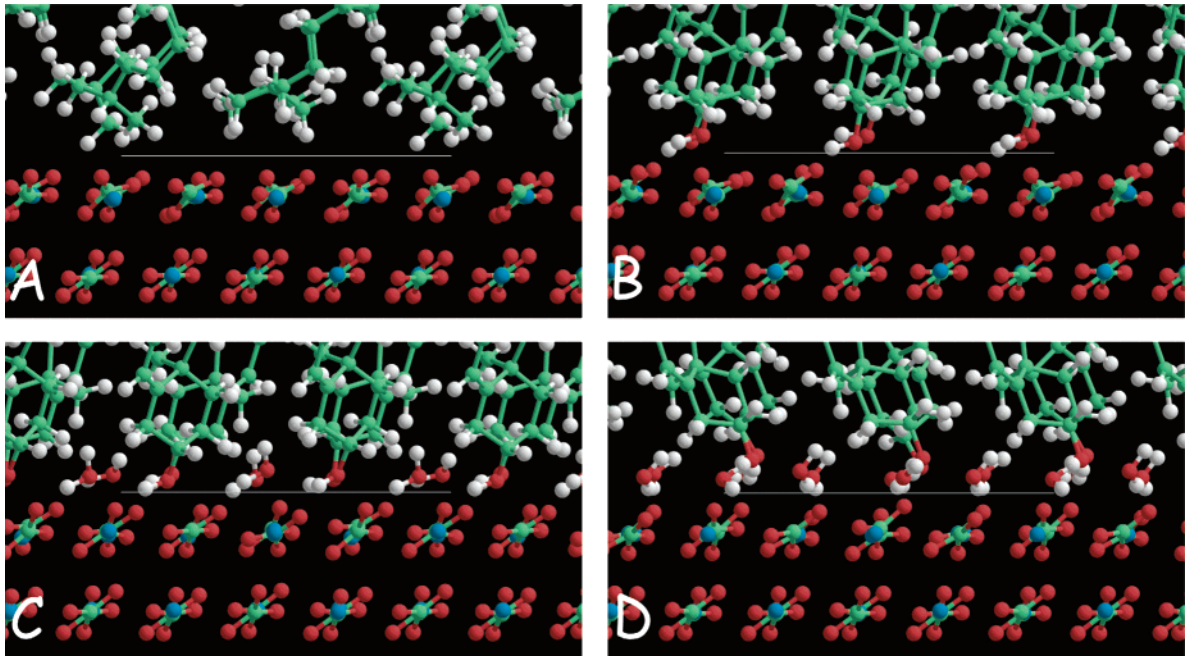

Figure 8. View of the optimized interfaces for the **ChM** (001) docked onto calcite ($10\bar{1}4$). A = hydrophobic **ChM**; B = hydrophilic **ChM**; C = hydrophilic **ChM** with a half hydration layer; D = hydrophilic **ChM** with a full hydration layer.

the (001) surface of a **ChM** crystal. This is perhaps not surprising because the cholesterol slices all have a dipole moment that will interact more strongly with the highly ionic calcite surface than with the organic cholesterol surface.

The final optimized configurations for the four different slabs are reproduced in Figure 7. Magnified images of the various cholesterol−calcite interfaces are shown in Figure 8. The surface termination of the slab that interacts least strongly with the calcite basal surface is the hydrophobic one. This is also the surface termination with the smallest difference in attachment energies between adding to a calcite crystal or a **ChM** crystal. This illustrates that the interactions between a hydrophobic surface and an ionic crystal are weak. As we move from the slab with a hydrophilic termination, to a half water layer termination, and finally from a slab with a full layer of water termination, there is an increase in the energy liberated upon attachment.

The hydrophilic terminated surface shows directional bonding with the calcite surface, in which the hydroxyl groups of the cholesterol molecules hydrogen bond to half of the surface carbonate anions (Figures 7 and 8B). The four unique H···O (O···O) distances are 1.500 (2.451), 1.504 (2.405), 1.540 (2.474), and 1.767 (2.462) Å with associated O−H···O angles of 148.2°, 158.0°, 154.8°, and 125.0°, respectively. Three of the four cholesterol molecules hydrogen bond very strongly to the surface, but the fourth one is unable to because even though the (001) face of cholesterol lattice matches the calcite basal plane well, there is still some residual lattice misfit.

When half a layer of water is present at the interface, a similar hydrogen bonding arrangement is observed between the hydroxyl groups of the cholesterol molecule and the surface carbonate anions. The water molecules are located in rows between the cholesterol hydroxyl groups (Figures 7 and 8C), which allow the hydroxyl groups of the cholesterol to get closer to the carbonate groups. The H···O (O···O) distances are now 1.460 (2.421), 1.469 (2.376), 1.524 (2.412), and 1.528 (2.471) Å with O−H···O angles of 159.4°, 148.6°, 146.1°, and 156.6°, respectively. The water molecules also hydrogen bond to a single carbonate group with distances of 1.510 (2.506), 1.521 (2.465), 1.524 (2.516), and 1.655 (2.541) Å and associated angles of 170.1°, 154.5°, 169.1°, and 146.2°, respectively. The second hydrogen atom on each water molecule projects into the hydrophobic areas above the hydroxyl groups of the cholesterol molecules. Thus, the water has improved the interaction energy between contacting surfaces, in essence acting as a screen between the calcite surface and the hydrophobic parts of the cholesterol molecule. The presence of a whole layer of water allows the hydroxyl groups of cholesterol to approach the carbonate ions of calcite still further (Figures 7 and 8D). The H···O (O···O) distances are now 1.411 (2.399), 1.414 (2.404), 1.507 (2.461), and 1.518 (2.464) Å with associated angles of 169.6°, 170.8°, 160.4°, and 158.5°, respectively. The additional water molecules are positioned in the same rows as the hydroxyl groups, with each water molecule lying between two cholesterol molecules.

Conclusions

There are presumably a variety of different mechanisms by which cholesterol nucleation can occur in complex biological solutions. In the present work, we have focused our attention solely on the potential influence that insoluble calcite seeds might play in the crystallization of cholesterol monohydrate. Using in situ AFM, we have demonstrated experimentally that the ($10\bar{1}4$) calcite surface can serve to catalyze the precipitation of cholesterol monohydrate from bile solutions under physiologic temperature conditions. Analysis of sequential images reveals that the evolution of these surface-bound **ChM** islands over time is a complex balance of individual island growth and Ostwald's ripening. However, the strong orientation and directional growth of all **ChM** islands provide unambiguous evidence that epitaxial matching at the calcite/cholesterol interface is an important factor. While the orientation observed matches the

values predicted in an earlier geometric lattice-matching study, the more rigorous molecular simulations of the $(10\bar{1}4)$ calcite/(001) **ChM** interfaces provide significantly greater insight into the energetics of that interface. Both geometric and chemical interactions influence the alignment of ions and molecules at the boundary of these two different crystalline materials. Perhaps not surprisingly, the presence of interfacial water molecules plays a key role in mediating the repulsive interactions associated with bringing ionic and neutral surfaces together. The dual theoretical and experimental approaches adopted in this study bring us closer to a molecular-scale understanding of at least one viable means by which the energetic barrier to cholesterol nucleation can be reduced under some physiological conditions.

Acknowledgment. J.A.S. is grateful for the financial support provided by the Henry Luce Foundation and the National Science Foundation (DMR-0093069). S.D.F. would like to acknowledge the Government of Western Australia for financial support under the Premier's Research Fellowship Program. A.L.R. would like to thank Dr. Stefano Piana for invaluable discussions.

Supporting Information Available: A table of coordinates for the minimized cholesterol monohydrate structure (CIF). This material is available free of charge via the Internet at http://pubs.acs.org.

JA0488030